ChemPubSoc Europe
DOI: 10.1002/chem.201504907
CHEMISTRY A European Journal
Full Paper

Structure Elucidation |*Hot Paper*|

# The Utilization of Amide Groups To Expand and Functionalize Metal–Organic Frameworks Simultaneously

Zhiyong Lu,[a, b] Junfeng Bai,*[a] Cheng Hang,[a] Fei Meng,[a] Wenlong Liu,[c] Yi Pan,[a] and Xiaozeng You[a]

**Abstract:** A new stepwise ligand-elongation strategy by amide spacers is utilized to prepare isoreticularly high-porous metal–organic frameworks (MOFs), namely, quasi-mesoporous $[Cu_2(PDBAD)(H_2O)]_n$ ($H_4PDBAD$ = 5,5′-((4,4′-((pyridine-3,5-dicarbonyl)bis(azanediyl))bis(benzoyl))bis(azanediyl))diisophthalic acid; NJU-Bai22: NJU-Bai for Nanjing University Bai's group), and mesoporous $[Cu_2(PABAD)(H_2O)]_n$ ($H_4PABAD$ = 5,5′-((4,4′-((4,4′-((pyridine-3,5-dicarbonyl)bis(azanediyl))bis(benzoyl))bis (azanediyl))bis(benzoyl))bis(azanediyl))diisophthalic acid; NJU-Bai23). Compared with the prototypical MOF of $[Cu_2(PDAD)(H_2O)]_n$ ($H_4PDAD$ = 5,5′-(pyridine-3,5-dicarbonyl)bis(azanediyl)diisophthalic acid; NJU-Bai21, also termed as PCN-124), both MOFs exhibit almost the same $CO_2$ adsorption enthalpy and $CO_2$ selectivity values, and better capacity for $CO_2$ storage under high pressure; these results make them promising candidate materials for $CO_2$ capture and sequestration. Interestingly, this new method, in comparison with traditional strategies of using phenyl or triple-bond spacers, is easier and cheaper, resulting in a better ability to retain high $CO_2$ affinity and selectivity in MOFs with large pores and high $CO_2$ storage capacity. Additionally, it may lead to the high thermal stability of the MOFs and also their tolerance to water, which is related to the balance between the density of functional groups and pore sizes. Therefore, this strategy could provide new opportunities to explore more functionalized mesoporous MOFs with high performance.

## Introduction

Global warming caused by rapid accumulation of $CO_2$ is of great concern for society as the main factor that causes climate change.[1] To eliminate $CO_2$ emission, great efforts have been dedicated to developing versatile $CO_2$ capture materials with low energy consumption, and a number of porous solids with good physical adsorption properties, such as zeolites and carbons,[2] have been intensively investigated. Recently, metal–organic frameworks (MOFs), emerging as a new type of material for $CO_2$ capture and sequestration (CCS), have attracted much interest due to their crystalline and modular nature in both organic and inorganic parts.[3]

[a] Dr. Z. Lu, Prof. Dr. J. Bai, C. Hang, F. Meng, Prof. Dr. Y. Pan, Prof. Dr. X. You
State Key Laboratory of Coordination Chemistry
Nanjing University, Nanjing 210093 (P.R. China)
E-mail: bjunfeng@nju.edu.cn

[b] Dr. Z. Lu
College of Mechanics and Materials
Hohai University, Nanjing 210098 (P.R. China)

[c] Prof. Dr. W. Liu
College of Chemistry and Chemical Engineering
Yangzhou University, Yangzhou 225002 (P.R. China)

*Supporting information and ORCID number from the author for this article are available on the WWW under http://dx.doi.org/10.1002/chem.201504907. It includes synthetic procedures, crystallographic tables, powder XRD and thermogravimetric data, additional gas adsorption isotherms, Langmuir and BET surface area analyses, pore size distributions, and details of the isosteric adsorption enthalpy and IAST calculations.*

The best and most efficient CCS material should possess both high storage capacity and high selectivity. However, the design of CCS materials is still a great challenge.[1a,3a] To meet these requirements, MOFs could serve as ideal platforms that are capable of being deliberately and finely tailored and functionalized on a molecular level. Several groups, including that of Yaghi, have made profound contributions to the design of MOFs with high $CO_2$ affinity and selectivity, such as attaching polar functional groups to organic ligands,[4] immobilizing nitrogen bases on open metal sites (OMSs),[5] impregnating metal irons,[6] and shrinking inner pores to adapt to the size of the $CO_2$ molecule.[7] Nevertheless, these precedents commonly face the problem of triggering a loss in the $CO_2$ storage capacity of the MOFs upon improving their $CO_2$ selectivity and, at the same time, encountering a barrier of diffusion due to smaller pores. On the other hand, if larger pores, mesopores for instance, as well as high $CO_2$ storage capacity are the main focus, which is generally exemplified by isoreticular expansion of MOFs through triple bonds or phenyl spacers,[8] the mass-transfer problem may be appropriately avoided, but a decline in $CO_2$ selectivity would be induced. Inserting amide groups into the skeleton of MOFs, as initiated by our group, is a promising approach for the functionalization of MOFs almost without compromising the surface area and porosity; this generates MOFs with high $CO_2$ selectivity and high $CO_2$ storage capacity.[9]

To further expand our work, and also inspired by the structures of proteins built upon repeating peptide bonds,[10] we

wondered if it was possible to use the amide group as a basic spacer in ligand elongation to further expand and functionalize isostructural MOFs under the guidance of the isoreticular principle.[11] Herein, a highly connected MOF with *txt* topology was chosen as a target platform for isoreticular syntheses due to its high stability as a results of high connectivity. Based upon a V-shaped ligand, 5,5′-(pyridine-3,5-dicarbonyl)bis(azanediyl)diisophthalic acid ($H_4$PDAD; Figure 1 a, $n=0$), by expanding the ligand with *para*-aminobenzoic acid (PAB) units (with amide groups embedded after the amidation reaction, as a semirigid skeleton that comprehensively mediates the conflict between isoreticular synthesis and flexibility[12]), isoreticular *txt*-type MOFs were successfully synthesized. Compared with the prototypical MOF NJU-Bai21 (NJU-Bai for Nanjing University Bai's group) synthesized from $H_4$PDAD, its extended analogues, quasi-mesoporous NJU-Bai22 and mesoporous NJU-Bai23, show much higher $CO_2$ storage capacity, but comparable $CO_2$ selectivity. This new way of ligand elongation, in contrast with traditional strategies of using phenyl or triple-bond spacers, can simultaneously realize pore expansion and functionalization, and provide better access to mesoporous MOFs with high $CO_2$ storage capacity, as well as good $CO_2$ affinity and selectivity. Meanwhile, some other problems caused by pure acetylene or phenyl groups, such as low solubility of ligands, complicated procedures, and high cost in synthesis, can be solved subsequently.

## Results and Discussion

### Synthesis and crystal structure

Preliminary exploratory reactions were based on solvothermal reactions between cupric nitrate and V-shaped ligands (Figure 1 a) in similar solvent systems. The reaction of $H_4$PDAD ($n=0$) and $Cu(NO_3)_2{\cdot}3H_2O$ in a mixture of DMF/$H_2O$ (5/1 v/v) containing $HNO_3$ afforded blue rhombic dodecahedral crystals of $[Cu_2(PDAD)(H_2O)]_n$, NJU-Bai21 (also termed as PCN-124[13]). Based upon $H_4$PDAD, ligands were elongated with one or two pairs of PAB units, and then $H_4$PDBAD (5,5′-((4,4′-((pyridine-3,5-dicarbonyl)bis(azanediyl))bis(benzoyl))bis(azane -diyl))diisophthalic acid) ($n=1$) and $H_4$PABAD (5,5′-((4,4′-((4,4′-((pyridine-3,5-dicarbonyl)bis(azanediyl))bis(benzoyl))bis (azanediyl))bis(benzoyl))bis(azanediyl))diisophthalic acid) ($n=2$; Figure 1 a and Scheme 1) were successfully synthesized. From these two ligands, $[Cu_2(PDBAD)(H_2O)]_n$ (NJU-Bai22) and $[Cu_2(PABAD)(H_2O)]_n$ (NJU-Bai23) were correspondingly obtained.

NJU-Bai21 crystallizes in cubic space group $Im\bar{3}m$. It exhibits a typical (3,36)-connected *txt* topology[14] (Figure 1 c) isostructural to that of Cu-DBPP[13], which is connected with triple-bond spacers instead. (For clarity, Cu-DBPP and PCN-124 were renamed as NJU-Bai20 and NJU-Bai21, respectively, in our incipient work for zero and one pair of amide groups in their ligands; and likewise for NJU-Bai22 and -Bai23 shown in Fig-

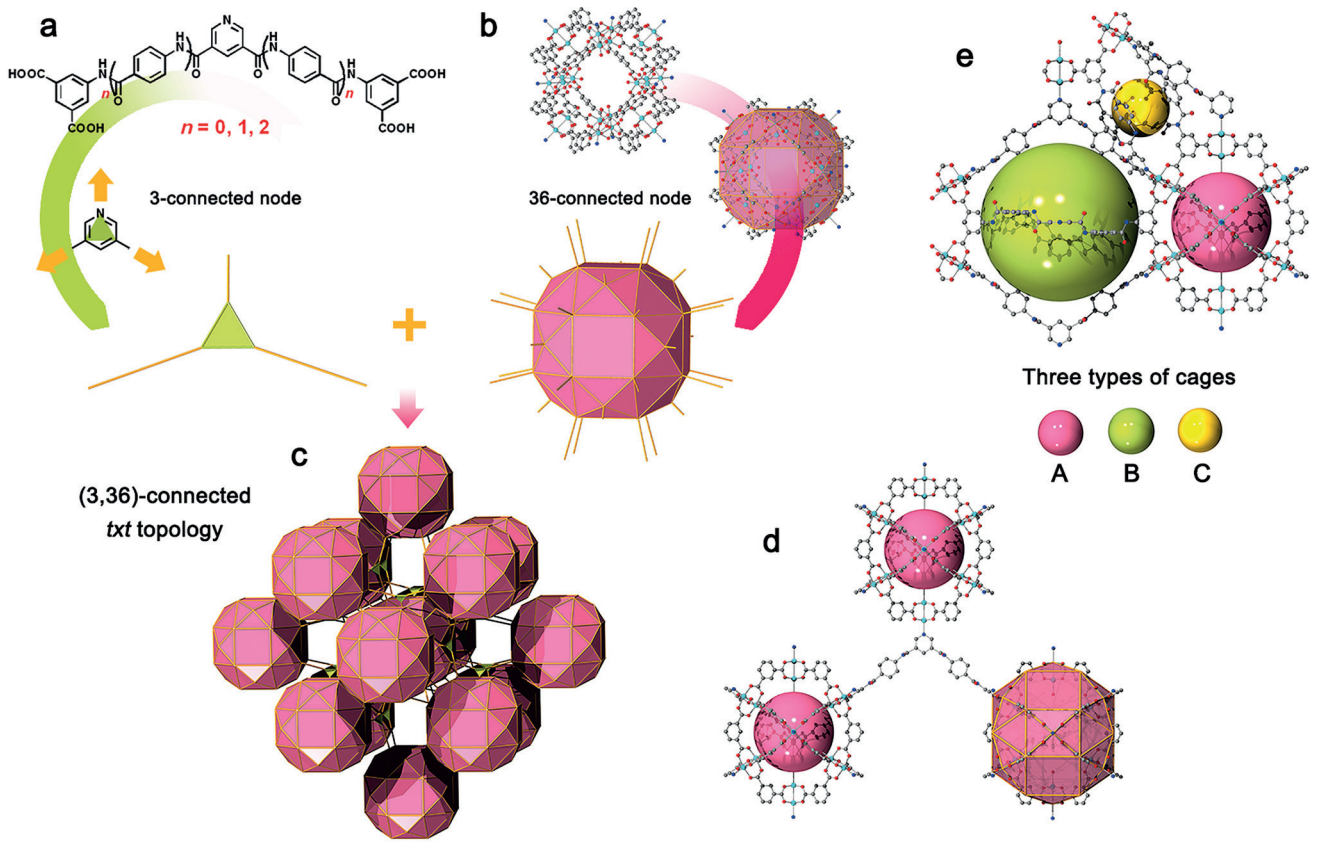


**Figure 1.** a) V-shaped ligand simplified as a three-connected node. b) Small rhombihexahedron cage simplified as a 36-connected node. c) The (3,36)-connected *txt* topology. d) Specific connections between the ligand and small rhombihexahedron cages. e) Three kinds of cages (or pores) and their packing mode.

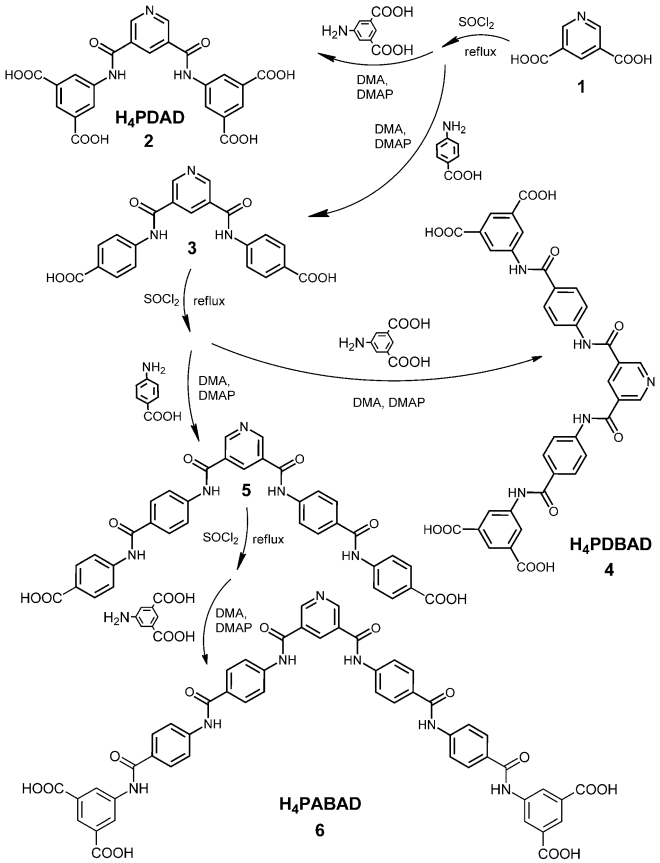


**Scheme 1.** The syntheses of $H_4$PDAD, $H_4$PDBAD, and $H_4$PABAD. DMA = *N*,*N*-dimethylacetamide, DMAP = 4-dimethylaminopyridine.

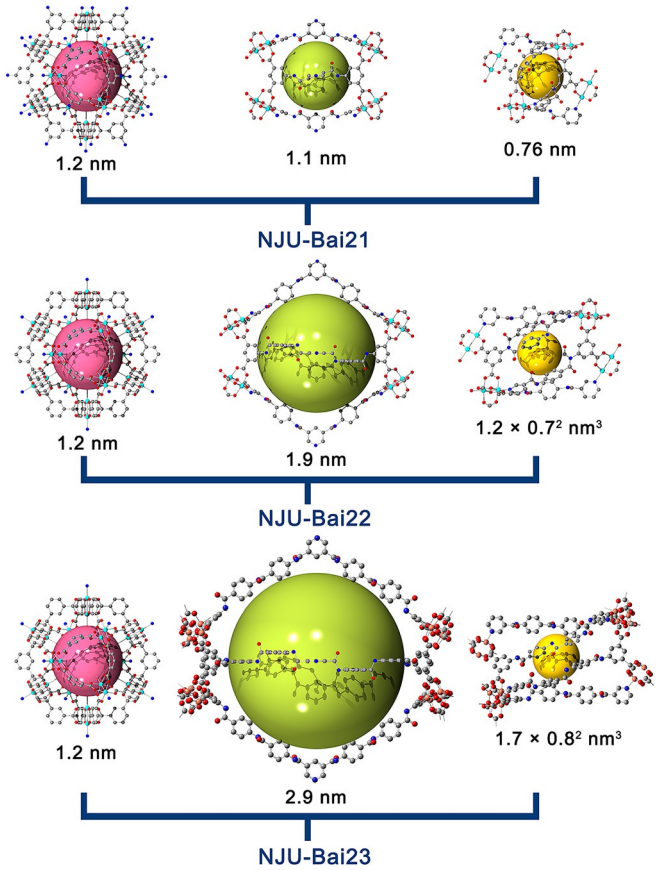


**Figure 2.** Isoreticular expansion of *txt*-type MOFs induces a variation in pore size from micro- to mesopores.

ure S7 in the Supporting Information.) Three types of cages (A, B, and C) exist in NJU-Bai21 with diameters of 1.2, 1.1, and 0.76 nm (Figure 2), respectively.

As an isostructural analogue of NJU-Bai21, NJU-Bai22 also crystallizes in cubic space group $Im\bar{3}m$, and the symmetric unit consists of one quarter of a PDBAD ligand, two crystallographically quarter $Cu^{2+}$ ions, and one quarter of a coordinated water molecule (Figure S8b in the Supporting Information). All copper clusters reveal a paddle-wheel-like shape, of which four equatorial sites are occupied by different benzene-1,3-dicarboxylate (bdc) moieties. One of the axial sites of the paddle-wheel is coordinated to the pyridyl nitrogen atom of the ligand, which makes the paddle-wheel a site for extension. Therefore, the small rhombihexahedron cage, widely known as a "nanoball",[15] is composed of 12 cupric paddle-wheel clusters and 24 bdc moieties; in total, this results in 36 points of extension (Figure 1). As expected, NJU-Bai22 exhibits the same *txt* topology (Figure 1 and Figure S7 in the Supporting Information), by simplifying ligands to 3-connnected nodes and nanoballs as 36-connected nodes. The overall structure also consists of three types of cages, cages A, B, and C, as shown in Figure 2. Two of them are strongly correlated with the size of the ligands. Thus, owing to ligand expansion, cage B is extended to a diameter of 1.9 nm, which is close to that of a mesopore, and cage C is inflated to $1.2\times0.7^2$ nm$^3$ (Figure 2). The inner cavity of NJU-Bai22 endows it with high porosity, as calculated by using the PLATON routine, with a solvent-accessible volume of 66.2% in the dehydrated structure of NJU-Bai22.

The isoreticular character of NJU-Bai21 and NJU-Bai22 reveals good consistency in isoreticular synthesis by the V-shaped ligands; thus the crystal structure of NJU-Bai23, with longer ligands, is assumed to be of the same type. In the shape of a rhombic dodecahedron, NJU-Bai23 crystallizes with a size of about $2\times2\times2$ mm$^3$. However, due to very weak diffraction, the single-crystal structure of NJU-Bai23 was not successfully obtained. To confirm the structure of NJU-Bai23, we loaded a single crystal of it onto an X-ray diffractometer with $Cu_{K\alpha}$ radiation for unit cell analysis; the values are listed in Table 1. The same crystal system and gradually increasing cell volumes after ligand elongation imply the isoreticular feature of NJU-Bai23 as being similar to those of NJU-Bai22 and -Bai21. Furthermore, the powder X-ray diffraction (PXRD) pattern of

**Table 1.** Crystal unit cell parameters obtained from single-crystal X-ray experiments.

| MOFs | Length of ligand [Å] | Crystal system | $a=b=c$ [Å] | $\alpha=\beta=\gamma$ [°] | $V$ [Å$^{-3}$] |
|---|---|---|---|---|---|
| NJU-Bai21 | 17 | cubic *I* | 30.41 | 90 | 28130 |
| NJU-Bai22 | 25 | cubic *I* | 38.72 | 90 | 58052 |
| NJU-Bai23 | 36 | cubic *I* | 46.03 | 90 | 97452 |

NJU-Bai23 was fully indexed and a LeBail profile fitting routine was performed by using the Rietica software ($Rp = 2.855\,\%$, $wRp = 4.977\,\%$); this resulted in a space group of $Im\bar{3}m$ with $a = 46.0307$ Å and $V = 97\,531.0$ Å$^3$ (Figure S10 in the Supporting Information). Clearly, crystal parameters obtained from the PXRD pattern coincide with that measured on the single-crystal X-ray diffractometer, which confirms the assumption of the structure of NJU-Bai23. Through a comparison of the PXRD patterns of NJU-Bai23, -Bai22, and -Bai21, as shown in Figure 3,

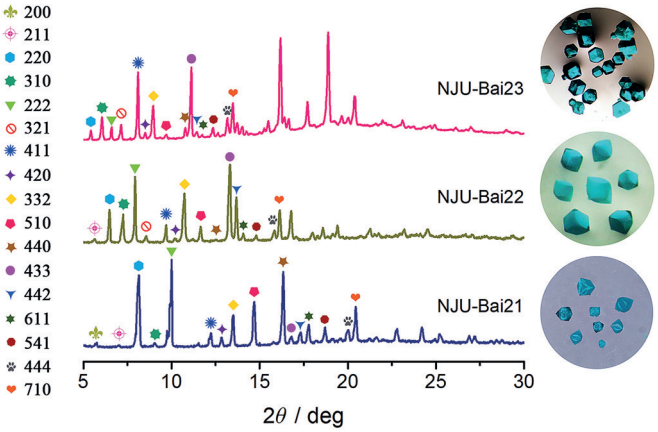


**Figure 3.** PXRD patterns and crystal-shape comparison of NJU-Bai21, -Bai22, and -Bai23.

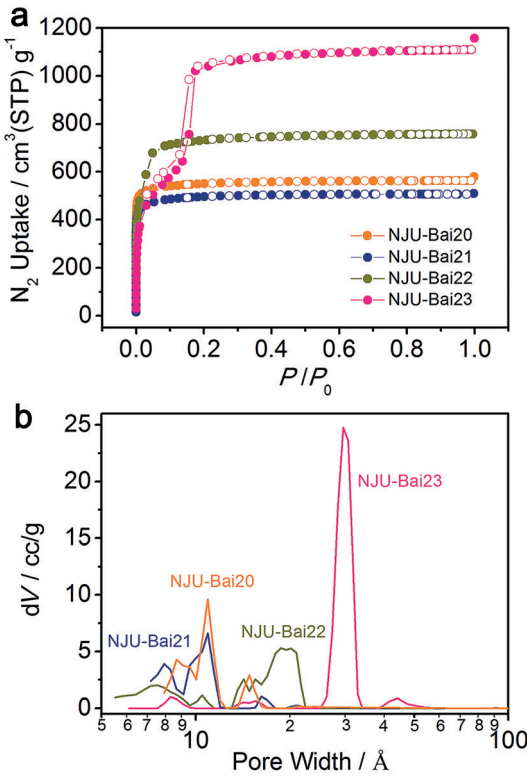


**Figure 4.** a) $N_2$ adsorption isotherms of NJU-Bai20, -Bai21, -Bai22, and -Bai23 at 77 K. b) PSDs in NJU-Bai20, -Bai21, -Bai22, and -Bai23.

shifting of the principal diffraction lines toward lower angles after ligand elongation indicates isoreticular crystal-lattice expansion. Similar shifting of PXRD peaks synchronous with ligand elongation is commonly observed in isoreticular MOFs;[8a,16] thus, to some extent, validating our inference about the crystal structure of NJU-Bai23. Meanwhile, a similar crystal shape also contributes perceptive evidence. Therefore, based upon the connectivity of NJU-Bai21 and -Bai22, the cage models of NJU-Bai23 were constructed by using GaussianView 3.0. As shown in Figure 2, cage B in NJU-Bai23 is extended to have a diameter of 2.9 nm and cage C is extended to $1.7 \times 0.8^2$ nm$^3$. The accuracy of these models and their pore apertures can be further confirmed by pore size distribution (PSD) analysis of NJU-Bai23 given in the following section, making NJU-Bai23 one of the mesoporous MOFs. Notably, the geometry of the main pore, cage B, gradually changes from fusiform in NJU-Bai21 to approximately spherical in NJU-Bai23, which may contribute to the mechanical stability of NJU-Bai23.

## Surface area and porosity

The permanent porosity of NJU-Bai22 and -Bai23 was confirmed by $N_2$ adsorption measurements at 77 K. As shown in Figure 4a, NJU-Bai22 exhibits a reversible pseudo-type I isotherm with a slight step before the plateau appears, which is typical in MOFs with both micro- and mesopores.[17] In contrast, NJU-Bai23 reveals distinctive step at $P/P_0 \approx 0.16$ with a clear hysteresis in its type IV isotherm, which is a characteristic of MOFs with hierarchically assembled mesopores.[8a,16d,18]

Similar behavior was also observed in the Ar isotherm of NJU-Bai23 at 87 K, as shown in Figure S19 in the Supporting Information. The occurrence of multilayer sorption in the large mesoporous cavities after surface coverage and small pore filling may explain this stepwise sorption behavior. The saturated nitrogen uptakes at 77 K in NJU-Bai22 and NJU-Bai23 are 758 and 1157 cm$^3$ g$^{-1}$, which feature high Langmuir surface areas of about 3299 and 5142 m$^2$ g$^{-1}$, respectively, if monolayer coverage of $N_2$ is assumed. Notably, the Langmuir surface area of NJU-Bai23 is comparable to that of MOF-177[19] (5340 m$^2$ g$^{-1}$), MIL-101c[20] (5900 m$^2$ g$^{-1}$), PCN-66[8c] (4600 m$^2$ g$^{-1}$), and PCN-68[8c] (6033 m$^2$ g$^{-1}$); this makes it a MOF with one of the highest surface areas. By applying the BET model, the apparent surface area of NJU-Bai22 was calculated to be 2177 m$^2$ g$^{-1}$. For NJU-Bai23, from the first plateau, the BET surface area was calculated to be 2519 m$^2$ g$^{-1}$. In contrast, NJU-Bai20 and NJU-Bai21 with smaller ligands exhibit total nitrogen uptakes of 580 and 510 cm$^3$ g$^{-1}$ (Figure 4a), with BET surface areas of 2221 and 1979 m$^2$ g$^{-1}$. The total pore volumes of NJU-Bai22 and -Bai23 obtained from $N_2$ isotherms ($P/P_0 = 0.976$) are 1.17 and 1.75 cm$^3$ g$^{-1}$, of which the latter is higher than that of some well-known mesoporous MOFs, such as MOF-177 (1.59 cm$^3$ g$^{-1}$), PCN-66 (1.36 cm$^3$ g$^{-1}$), and NOTT-112[17a] (1.62 cm$^3$ g$^{-1}$). Based on the Ar adsorption isotherm of NJU-Bai22 at 87 K (Figure S19 in the Supporting Information), PSD analysis by nonlocal density functional theory (NLDFT) methods shows that there are distributions of micropores at 0.6–0.9 and 1.1–1.2 nm, and quasi-mesopores at 1.5–2.1 nm (Fig-

ure 4 b), which coincides with the three types of cages observed in the crystal structure of NJU-Bai22. To test the reliability of the NLDFT mode, the pore distributions of NJU-Bai20 and -Bai21 were also analyzed; all results were in good accordance with pore sizes measured in their crystal structures (Figure 2 and Figure S6 in the Supporting Information). Then, for NJU-Bai23, the same analysis method was applied, and the pore sizes were distributed among 0.7–0.9, 1.5–1.7, and around 2.9 nm (Figure 4 b). Clearly, these results are consistent with the pores we built for NJU-Bai23; therefore, the crystal structure of NJU-Bai23 and its mesoporous characteristic can be confirmed.

### $CO_2$ adsorption properties and selectivities

To investigate the influence of ligand elongation by amide spacers on $CO_2$ uptake capacity, we continued to measure the $CO_2$ adsorption behavior of these analogues at 273 and 298 K. It is our preconception that the $CO_2$ affinities and selectivities of the two new isoreticular analogues should be almost the same as that of NJU-Bai21 and much higher than that of NJU-Bai20 without amide groups. Like the results demonstrated in our previous work,[9a,b,e–g] the introduction of amide spacers in NJU-Bai21 significantly improves $CO_2$ adsorption (206.5 $cm^3 g^{-1}$ at 273 K and 1 bar and 115.1 $cm^3 g^{-1}$ at 298 K and 1 bar), compared with NJU-Bai20 with triple-bond spacers (136.4 $cm^3 g^{-1}$ at 273 K and 1 bar and 68.0 $cm^3 g^{-1}$ at 298 K and 1 bar; Figure 5 a and b). Correspondingly, the $CO_2$ adsorption enthalpy shows a clear increase, from 22.2 $kJ mol^{-1}$ for NJU-Bai20 to 25.9 $kJ mol^{-1}$ for NJU-Bai21, with zero coverage (Figure 5 c). For NJU-Bai22 and -Bai23 with longer ligands, although gradual decreases in $CO_2$ adsorption relative to NJU-Bai21 (72.9 $cm^3 g^{-1}$ for NJU-Bai22 and 49.0 $cm^3 g^{-1}$ for NJU-Bai23 at 298 K and 1 bar) were observed, which is a common phenomenon after pore expansion,[19,8c] slight bending along the *y* axis in the curve of the adsorption isotherms indicates strong interactions between $CO_2$ molecules and the framework. As illustrated in Figure 5 c, the zero-coverage $CO_2$ adsorption enthalpies of NJU-Bai22 and NJU-Bai23 were calculated to be 25.6 and 25.1 $kJ mol^{-1}$, respectively. Both values are close to that of NJU-Bai21 and much higher than that of NJU-Bai20; this implies that the strong $CO_2$ affinity of the frameworks can be retained after ligand elongation with repeated amide spacers.

Because the utilization of amide spacers can largely retain the adsorption enthalpy of $CO_2$, we further investigated the $CO_2$ selectivities of the four isoreticular analogues. As shown in Figures S28–S31 in the Supporting Information, the $CH_4$ and $N_2$ adsorption isotherms of NJU-Bai20, -Bai21, -Bai22, and -Bai23 were collected at 298 K. Although the $CO_2$ adsorption capacity declines upon ligand elongation, the $N_2$ and $CH_4$ adsorptions also show similar tendencies. Initially, the amount of $CH_4$ uptake of NJU-Bai21 at 1 bar is 20.3 $cm^3 g^{-1}$. After ligand elongation with one unit, NJU-Bai22 can only adsorb 16.1 $cm^3 g^{-1}$ of $CH_4$. With ligand elongated by two units, the amount of $CH_4$ uptake of NJU-Bai23 decreases to 11.9 $cm^3 g^{-1}$. Similar behavior was also observed in the $N_2$ uptakes, from 4.82 $cm^3 g^{-1}$ in NJU-Bai21 to 4.07 $cm^3 g^{-1}$ in NJU-Bai22 and 2.52 $cm^3 g^{-1}$ in NJU-Bai23. This consistency may lead to the invariability of $CO_2$ selectivity. Thus, based upon experimental $CO_2$, $CH_4$, and $N_2$ isotherms, the $CO_2$ selectivities of NJU-Bai21, -Bai22, and -Bai23 were calculated by means of simplified ideal adsorption solution theory (IAST), which serves as the benchmark for the sim-

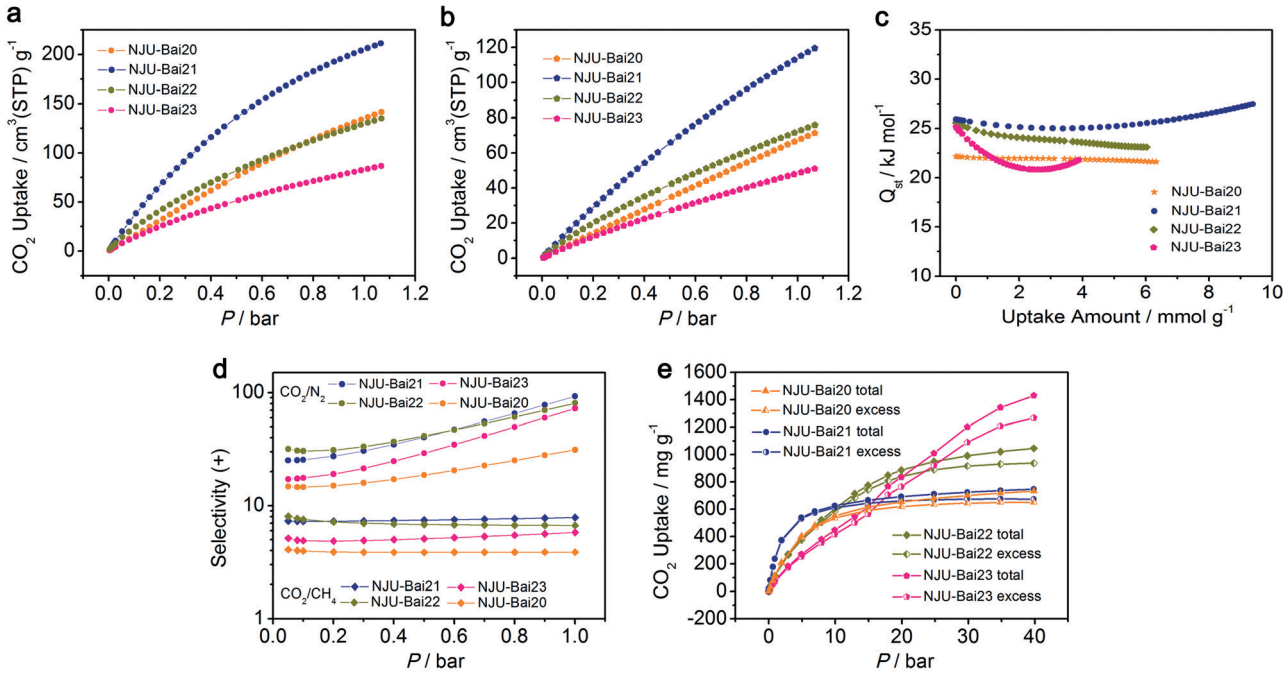


**Figure 5.** $CO_2$ adsorption isotherms of NJU-Bai20, -Bai21, -Bai22, and -Bai23 at 273 (a) and 298 K (b). c) $CO_2$ adsorption enthalpies of NJU-Bai20, -Bai21, -Bai22, and -Bai23. d) The selectivities of $CO_2$ over $N_2$ and $CH_4$ of NJU-Bai20, -Bai21, -Bai22, and -Bai23. e) $CO_2$ adsorption isotherms of NJU-Bai20, -Bai21, -Bai22, and -Bai23 in the high-pressure range.

ulation and computational analysis of binary mixture adsorption from experimental isotherms.[1a,21] The adsorption selectivity is defined as $S_{i/j}=(q_1/q_2)/(p_1/p_2)$, in which $q_i$ is the amount of i adsorbed and $p_i$ is the partial pressure of i in the mixture. As shown in Figure 5 d, at 1 bar in a binary mixture of $CO_2$ and $N_2$ with a ratio of 15:85, the predicted $CO_2/N_2$ selectivities of NJU-Bai21, -Bai22, and -Bai23 are 93, 81, and 72, respectively. In an equimolar gas-phase mixture of $CO_2$ and $CH_4$, the $CO_2$ selectivities of NJU-Bai21, -Bai22, and -Bai23 are 7.8, 6.7, and 5.8, respectively. Clearly, ligand expansion does not cause a drastic decline in $CO_2$ selectivity against $N_2$ and $CH_4$. Given that the $CO_2/N_2$ and $CO_2/CH_4$ selectivities of NJU-Bai23 show a slight decrease compared with that of NJU-Bai21, they are still about two times that of NJU-Bai20 without amide groups ($CO_2/N_2$: 31, $CO_2/CH_4$: 3.9) and significantly higher than that of some well-known MOFs, such as CuBTC ($CO_2/N_2$: 21, $CO_2/CH_4$: 5),[22] bio-MOF-11 ($CO_2/N_2$: 36),[22,23] Cu-TPBTM ($CO_2/N_2$: 21)[9f] and MOF-177 ($CO_2/N_2$:5, $CO_2/CH_4$:4.4),[24] as shown in Table S3 in the Supporting Information. The high selectivities of $CO_2$ over $N_2$ and $CH_4$ in these three isoreticularly amide-decorated MOFs suggest their possible application in capturing $CO_2$ from flue gas or upgrading natural gas; meanwhile, these MOFs are also rare examples of retaining good $CO_2$ selectivity in mesoporous MOFs.

Ligand elongation in the isoreticular synthesis of NJU-Bai21 not only generates large pores, mesopores for instance, but also retains good affinity for $CO_2$ molecules and good $CO_2$ selectivity. This phenomenon should be mainly due to retaining the density of functional groups. It is widely acknowledged that OMSs are a distinct type of binding sites preferred by $CO_2$ molecules.[25] Together with the amide groups, classified as Lewis base sites (LBSs), two main kinds of binding sites for $CO_2$ molecules exist in the three amide-decorated analogues NJU-Bai21, -Bai22, and -Bai23. As the cell volume increases gradually, the amount of OMSs remains constant, whereas the quantity of LBSs almost doubles. Thus, the density of functional groups only shows a small decline (from 2.5 $nm^{-3}$ to 2.1 and 1.7 $nm^{-3}$), although a steep increase in cell volume occurs, which contributes to the slight decline in $CO_2$ adsorption enthalpy. Assuming that the amide spacers of these amide-decorated analogues were substituted by phenyl or triple-bond spacers and their cell volumes almost remained constant, similar to the traditional method of ligand elongation without LBSs, the densities of functional groups in the substitutes would be far lower than those of their prototypes (Table 2), which would make the $CO_2$ affinities and selectivities of substitutes for NJU-Bai22 and -Bai23 even lower than that of a substitute of NJU-Bai21, namely, NJU-Bai20.

Bearing in mind the large pores we obtained, and the good $CO_2$ enthalpies and selectivities resulting from the amide spacers, we further measured the $CO_2$ storage capacity of the four isoreticular analogues at 298 K under high pressure. As shown in Figure 5 e, although NJU-Bai21 possesses a lower surface area and pore volume than NJU-Bai20, a higher $CO_2$ uptake amount was observed in NJU-Bai21, especially between 0 and about 10 bar. According to common sense, a larger surface area and pore volume will guarantee a better gas storage capacity; however, herein there is a contradiction, which implies that the amide groups promote $CO_2$ storage. After elongating the ligands by one unit, NJU-Bai22 shows a higher excess $CO_2$ uptake of 937 mg $g^{-1}$ (48.4 wt%) at 40 bar. If gaseous $CO_2$ compressed within the pore void is taken into consideration, the total $CO_2$ uptake is 1046 mg $g^{-1}$ (51.5 wt%) at 40 bar. This value is larger than those of Cu-TDPAT[26] (892 mg $g^{-1}$, $S_{BET}=1938$ $m^2 g^{-1}$), IRMOF-6[1b] (858 mg $g^{-1}$, $S_{BET}=2516$ $m^2 g^{-1}$), MIL-100(Cr)[27] (792 mg $g^{-1}$, $S_{BET}=1900$ $m^2 g^{-1}$), IRMOF-11[1b] (647 mg $g^{-1}$, $S_{BET}=2096$ $m^2 g^{-1}$), and HKUST-1[1b] (40.1 *wt*%, $S_{BET}=2211$ $m^2 g^{-1}$), with a comparative surface area to NJU-Bai22. For NJU-Bai23, it is not yet saturated when the pressure reaches 40 bar. At this pressure, the excess $CO_2$ uptake amount is 1268 mg $g^{-1}$ (55.9 wt%) and the total $CO_2$ uptake is 1430 mg $g^{-1}$ (58.9 wt%). Although the total $CO_2$ uptake of NJU-Bai23 is much lower than that of some MOFs with extremely high surface areas, such as MOF-210 and MOF-200,[19] it is still comparable to those of MOF-177[19] (1356 mg $g^{-1}$, $S_{BET}=4500$ $m^2 g^{-1}$) and MOF-205[19] (1495 mg $g^{-1}$, $S_{BET}=4460$ $m^2 g^{-1}$); even NJU-Bai23 has a much lower BET surface area. Interestingly, the $CO_2$ adsorption isotherm of NJU-Bai23 shows two distinct steps at $P=15$ and $P=25$ bar without hysteresis, whereas NJU-Bai22 shows a slight step at $P=12$ bar in its $CO_2$ adsorption isotherm. This may be correlated to flexibility induced by the amide groups. When $CO_2$ molecules fill the pores under high pressure, the PAB moieties begin to rotate to adapt to the congested environment caused by $CO_2$ molecules. Because the ligands of NJU-Bai22 and NJU-Bai23 are expanded by one and two pairs of PAB units, respectively, their $CO_2$ adsorption isotherms under high pressure reveal one and two steps correspondingly. Therefore, the reasonability of the structural assumption for NJU-Bai23 is again confirmed.

**Table 2.** Density of functional groups in NJU-Bai21, -Bai22, -Bai23, and their hypothetical isostructural counterparts with phenyl or triple-bond spacers.

| MOFs | $V$ [$Å^{-3}$] | $N_{OMS}$[b] | $N_{LBS}$[c] | $D_F$[d] [$nm^{-3}$] |
|---|---|---|---|---|
| NJU-Bai21 | 28130 | 24 | 48 | 2.5 |
| NJU-Bai22 | 58052 | 24 | 96 | 2.1 |
| NJU-Bai23 | 97452 | 24 | 144 | 1.7 |
| NJU-Bai21-P/T[a] | 28130 | 24 | 0 | 0.85 |
| NJU-Bai22-P/T | 58052 | 24 | 0 | 0.4 |
| NJU-Bai23-P/T | 97452 | 24 | 0 | 0.24 |

[a] P/T indicates isostructural MOFs with phenyl or triple-bond spacers instead of amide spacers. [b] Amount of OMSs per unit cell. [c] Amount of LBSs per unit cell. [d] $D_F$ = density of functional groups.

### Thermal and water stability

Due to the high connectivity of this kind of (3,36)-connected MOFs, we further investigated the stability. A large quantity of bulk materials was prepared and applied in thermal stability and water stability measurements. The purity of the bulk materials has been demonstrated by the good agreement between the PXRD patterns and simulated patterns from single-crystal

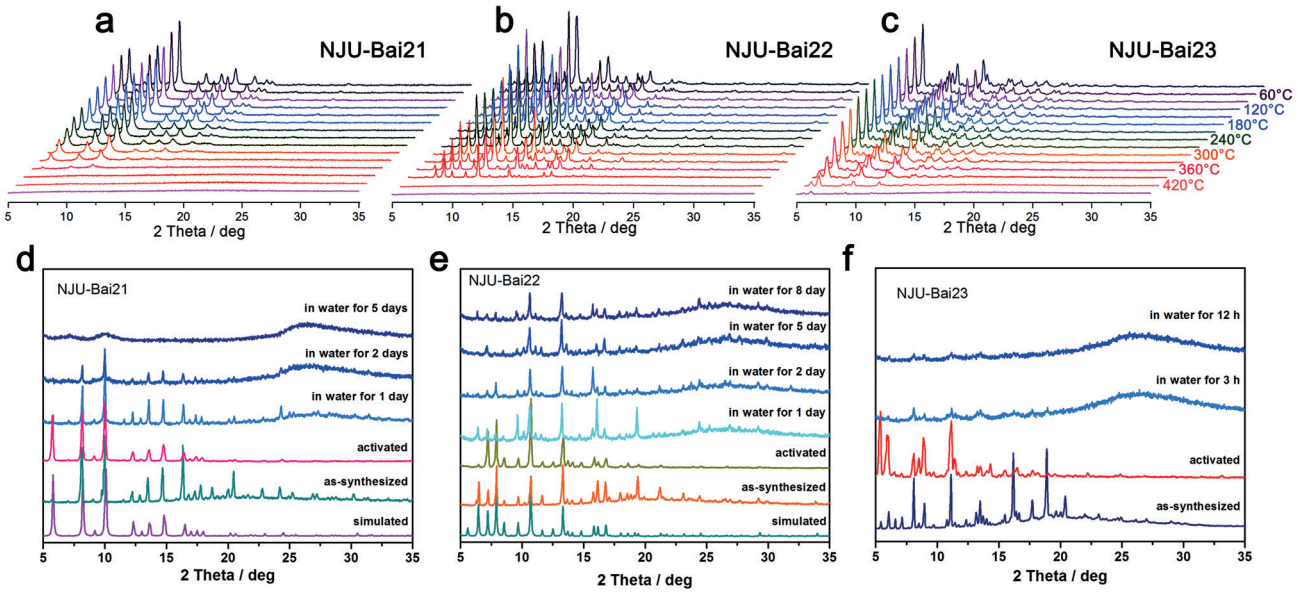


**Figure 6.** Variable-temperature (VT) PXRD patterns of activated samples of NJU-Bai21 (a), -Bai22 (b), and -Bai23 (c) under vacuum. The temperature increased by 30 °C from 30 to 450 °C. Results of water stability tests for NJU-Bai21 (d), -Bai22 (e), and -Bai23 (f), respectively.

data (Figure 6 d–f). Each sample was divided into two parts: the activated one for VT-PXRD measurements in vacuum (Figure 6 a–c) and the as-synthesized one for VT-PXRD measurement in vacuum (Figures S39–S42 in the Supporting Information). As shown in Figure 6, the structural compactness of the whole framework endows this type of MOF with good thermal stability. For NJU-Bai21, a shifting of PXRD peaks to higher angles was observed at 300 °C, which indicated flexibility of the whole structure at high temperature; this later induced structural collapse. For NJU-Bai22, no similar behavior was observed and it retained its structure below 390 °C. After expansion of ligands by two units, the activated sample of NJU-Bai23 can be stable up to 420 °C, although the as-synthesized sample easily collapses under vacuum due to the evacuation of solvent molecules (Figure S42 in the Supporting Information). For an activated sample of NJU-Bai23, longer ligands make the main pores (cage B) more approximately spherical, which is stable from a mechanical perspective. Thus, without the interruption of solvent molecules, NJU-Bai23 exhibits higher thermal stability than that of NJU-Bai21 and NJU-Bai22. However, if solvent molecules exist, surface tension caused by their evacuation would easily lead to the distortion of ligands, especially for longer ligands, as illustrated in Figure S36 in the Supporting Information, and then structural collapse is triggered, as exemplified by the as-synthesized sample of NJU-Bai23. Therefore, for the activated sample as the main form in practical applications, longer ligands endow this type of MOF with higher thermal stability, as also demonstrated by thermogravimetric analysis (TGA; Figures S32–S35 in the Supporting Information).

When water stability tests were conducted, the as-synthesized samples were directly immersed in fresh water and PXRD patterns were collected every 12 h (Figure 6 d–f). NJU-Bai20 shows the best water stability and its structure can be retained for more than one week in water (Figure S38 in the Supporting Information). This good performance can be attributed to two factors. First, half of the axial sites of copper paddle wheels are occupied by pyridyl groups with Cu–N bonds, which are stronger bonds than Cu–O bonds.[3a] When water molecules attack metal clusters, strong bonds ensure better resistance. Second, the hydrophobic acetylene groups in the ligands provide a hydrophobic environment in the pores. In this respect, if the hydrophobic moieties are substituted by some polar functional groups to improve the affinity for specific gases, as exemplified by NJU-Bai21, NJU-Bai22, and NJU-Bai23 with amide groups, the water stability will be weakened. Therefore, NJU-Bai21 can only maintain its structure for 36 h and NJU-Bai23 can last no longer than 3 h. Surprisingly, the water stability of NJU-Bai22 is comparable to that of NJU-Bai20, and much better than those of NJU-Bai21 and NJU-Bai23. NJU-Bai22 is able to maintain its structure for eight days, although part of it collapses into an amorphous state. To explain this phenomenon, two factors should be discussed: the density of the functional groups and pore sizes. A higher density of functional groups means that water molecules are attracted more easily, which causes the breakdown of the whole framework. Meanwhile, large pores permit free shuttling of water molecules; this raises the possibility of water molecules attacking metal clusters. NJU-Bai22, which possesses a moderate density of functional groups and suitable pore sizes, therefore, exhibits the best water stability of the three amide-decorated analogues.

## Conclusion

We systematically used amide groups for ligand elongation and MOF functionalization simultaneously, and successfully synthesized quasi-mesoporous NJU-Bai22 and mesoporous NJU-Bai23. In contrast with prototypical NJU-Bai21, although

the pore apertures in NJU-Bai22 were expanded to the quasi-mesoporous scale, the $CO_2$ adsorption enthalpy and selectivity remained almost constant, although the $CO_2$ storage capacity improved. Furthermore, the high thermal and water stability make it a promising candidate for CCS. After further expansion, mesoporous NJU-Bai23 still exhibits comparable $CO_2$ adsorption enthalpy and selectivity, with an even higher $CO_2$ storage capacity and higher thermal stability, but it is vulnerable to attack from water. NJU-Bai23 is a rare example of a mesoporous MOF that exhibits a high $CO_2$ storage capacity and high $CO_2$ selectivity. The strategy of isoreticular expansion by amide spacers may provide a new way to simultaneously expand the pores and functionalize MOFs. Moreover, compared with traditional strategies, it is easier and cheaper and performs better at retaining the $CO_2$ affinity and selectivity of MOFs with large pores and high $CO_2$ storage capacity. Therefore, continuous work to obtain *txt* or other types of MOFs with even larger pores is still ongoing.

## Experimental Section

### General

All chemical reagents were obtained from commercial sources and, unless otherwise noted, were used as received without further purification. $^1$H NMR spectra were recorded on a Bruker DRX-500 spectrometer with tetramethylsilane (TMS) as an internal reference. Elemental analyses (C, H, and N) were performed on a PerkinElmer 240 analyzer. The IR spectra were recorded in the range of $\tilde{\nu}=$ 400–4000 cm$^{-1}$ on a VECTOR TM 22 spectrometer as KBr pellets. PXRD data were collected on a Bruker D8 ADVANCE X-ray diffractometer, at 40 kV, 40 mA, with $Cu_{K\alpha}$ radiation, equipped with a variable-temperature stage and a vacuum system, with a scan speed of 0.1 s$^{\circ-1}$. The sample was held at the designated temperature for at least 10 min between each scan. TGA was performed under an $N_2$ atmosphere (100 mL min$^{-1}$) at a heating rate of 5 °C min$^{-1}$ by using a 2960 SDT thermogravimetric analyzer. MOF supercritical $CO_2$ drying was performed by using a Tousimis™ Samdri® PVT-30 critical point dryer (Tousimis, Rockville, MD, USA).

### Syntheses of ligands

Details of the synthesis of $H_4$PDAD (**2**), two new ligands $H_4$PDBAD (**4**) and $H_4$PABAD (**6**), and $H_4$PDED are given in the Supporting Information.

### Gas adsorption

Low-pressure gas sorption measurements were conducted by using a Micrometritics ASAP 2020 surface area and pore size analyzer up to saturated pressure at different temperatures. High-pressure gravimetric $CO_2$ adsorption measurements were performed on an ISOSORP HyGpra + V adsorption analyzer (Rubotherm, Germany) over the 0–40 bar range at 298 K. Before the gas sorption measurements, more than 400 mg (about 100 mg for high-pressure gas adsorption) of as-synthesized samples of NJU-Bai20, NJU-Bai21, and NJU-Bai22 were washed with DMF and methanol. Fresh anhydrous methanol was then added and the samples were allowed to soak for 3 days for solvent exchange. During this period, methanol was refreshed every 8 h. Each sample was then charged into a sample tube and activated at different temperatures (120, 80, and 100 °C for NJU-Bai20, NJU-Bai21, and NJU-Bai22, respectively) for 20 h under vacuum. For NJU-Bai23, the as-synthesized sample was washed with DMF three times and then soaked in anhydrous methanol for 3 days for solvent exchange. The sample was then activated by supercritical $CO_2$ (SCD) and then dried again under vacuum for 6 h at 60 °C prior to gas adsorption/desorption measurements. PSD was calculated from analysis of the Ar isotherm (adsorption branch) at 87 K by using NLDFT, which implemented a hybrid kernel based on a zeolite/silica model containing cylindrical pores in the software package of Quantachrome AUTOSORB-1 automatic volumetric instrument.

The wt % gas uptake is defined by Equation (1):

$$\text{wt}\,\% = (100 \times N)/(1000 + N) \quad (1)$$

in which $N$ is excess (or total) adsorption ($N_{exc}$ or $N_{tot}$, mg g$^{-1}$).

## Acknowledgements

We are grateful for support of this work by the Natural Science Foundation of China (21371091, 21371150).

**Keywords:** amides · isoreticular synthesis · mesoporous materials · metal–organic frameworks · structure elucidation

[1] a) D. M. D'Alessandro, B. Smit, J. R. Long, *Angew. Chem. Int. Ed.* **2010**, *49*, 6058–6082; *Angew. Chem.* **2010**, *122*, 6194–6219; b) A. R. Millward, O. M. Yaghi, *J. Am. Chem. Soc.* **2005**, *127*, 17998–17999.
[2] a) N. Hedin, L. Chen, A. Laaksonen, *Nanoscale* **2010**, *2*, 1819–1841; b) O. Cheung, N. Hedin, *RSC Adv.* **2014**, *4*, 14480–14494; c) J. Wei, D. Zhou, Z. Sun, Y. Deng, Y. Xia, D. Zhao, *Adv. Funct. Mater.* **2013**, *23*, 2322–2328.
[3] a) K. Sumida, D. L. Rogow, J. A. Mason, T. M. McDonald, E. D. Bloch, Z. R. Herm, T. H. Bae, J. R. Long, *Chem. Rev.* **2012**, *112*, 724–781; b) Z. Zhang, Z.-Z. Yao, S. Xiang, B. Chen, *Energy Environ. Sci.* **2014**, *7*, 2868–2899; c) W. Lu, W. M. Verdegaal, J. Yu, P. B. Balbuena, H.-K. Jeong, H.-C. Zhou, *Energy Environ. Sci.* **2013**, *6*, 3559–3564; d) S. Horike, K. Kishida, Y. Watanabe, Y. Inubushi, D. Umeyama, M. Sugimoto, T. Fukushima, M. Inukai, S. Kitagawa, *J. Am. Chem. Soc.* **2012**, *134*, 9852–9855; e) T.-H. Bae, M. R. Hudson, J. A. Mason, W. L. Queen, J. J. Dutton, K. Sumida, K. J. Micklash, S. S. Kaye, C. M. Brown, J. R. Long, *Energy Environ. Sci.* **2013**, *6*, 128–138; f) O. Shekhah, Y. Belmabkhout, Z. Chen, V. Guillerm, A. Cairns, K. Adil, M. Eddaoudi, *Nat. Commun.* **2014**, *5*, 4228.
[4] a) R. Banerjee, H. Furukawa, D. Britt, C. Knobler, M. O'Keeffe, O. M. Yaghi, *J. Am. Chem. Soc.* **2009**, *131*, 3875–3877; b) H. Deng, C. J. Doonan, H. Furukawa, R. B. Ferreira, J. Towne, C. B. Knobler, B. Wang, O. M. Yaghi, *Science* **2010**, *327*, 846–850; c) W. Morris, B. Leung, H. Furukawa, O. K. Yaghi, N. He, H. Hayashi, Y. Houndonougbo, M. Asta, B. B. Laird, O. M. Yaghi, *J. Am. Chem. Soc.* **2010**, *132*, 11006–11008; d) Y.-S. Bae, O. K. Farha, J. T. Hupp, R. Q. Snurr, *J. Mater. Chem.* **2009**, *19*, 2131–2134; e) T. Gadzikwa, O. K. Farha, K. L. Mulfort, J. T. Hupp, S. T. Nguyen, *Chem. Commun.* **2009**, 3720–3722; f) Y. Zhao, H. Wu, T. J. Emge, Q. Gong, N. Nijem, Y. J. Chabal, L. Kong, D. C. Langreth, H. Liu, H. Zeng, J. Li, *Chem. Eur. J.* **2011**, *17*, 5101–5109; g) Z. Chen, S. Xiang, H. D. Arman, P. Li, D. Zhao, B. Chen, *Eur. J. Inorg. Chem.* **2011**, 2227–2231; h) Z. Chen, S. Xiang, H. D. Arman, J. U. Mondal, P. Li, D. Zhao, B. Chen, *Inorg. Chem.* **2011**, *50*, 3442–3446.
[5] a) T. M. McDonald, D. M. D'Alessandro, R. Krishna, J. R. Long, *Chem. Sci.* **2011**, *2*, 2022–2028; b) T. M. McDonald, W. R. Lee, J. A. Mason, B. M. Wiers, C. S. Hong, J. R. Long, *J. Am. Chem. Soc.* **2012**, *134*, 7056–7065.
[6] a) H. J. Park, M. P. Suh, *Chem. Sci.* **2013**, *4*, 685–690; b) Y.-S. Bae, B. G. Hauser, O. K. Farha, J. T. Hupp, R. Q. Snurr, *Microporous Mesoporous Mater.* **2011**, *141*, 231–235.
[7] a) P. Nugent, Y. Belmabkhout, S. D. Burd, A. J. Cairns, R. Luebke, K. Forrest, T. Pham, S. Ma, B. Space, L. Wojtas, M. Eddaoudi, M. J. Zaworotko,

*Nature* **2013**, *495*, 80 – 84; b) S. D. Burd, S. Ma, J. A. Perman, B. J. Sikora, R. Q. Snurr, P. K. Thallapally, J. Tian, L. Wojtas, M. J. Zaworotko, *J. Am. Chem. Soc.* **2012**, *134*, 3663 – 3666; c) T. K. Prasad, M. P. Suh, *Chem. Eur. J.* **2012**, *18*, 8673 – 8680; d) L. Du, Z. Lu, K. Zheng, J. Wang, X. Zheng, Y. Pan, X. You, J. Bai, *J. Am. Chem. Soc.* **2013**, *135*, 562 – 565.

[8] a) O. K. Farha, I. Eryazici, N. C. Jeong, B. G. Hauser, C. E. Wilmer, A. A. Sarjeant, R. Q. Snurr, S. T. Nguyen, A. O. Yazaydin, J. T. Hupp, *J. Am. Chem. Soc.* **2012**, *134*, 15016 – 15021; b) H. Furukawa, K. E. Cordova, M. O'Keeffe, O. M. Yaghi, *Science* **2013**, *341*, 1230444; c) D. Yuan, D. Zhao, D. Sun, H. C. Zhou, *Angew. Chem. Int. Ed.* **2010**, *49*, 5357 – 5361; *Angew. Chem.* **2010**, *122*, 5485 – 5489.

[9] a) J. Duan, Z. Yang, J. Bai, B. Zheng, Y. Li, S. Li, *Chem. Commun.* **2012**, *48*, 3058 – 3060; b) Z. Y. Lu, H. Xing, R. Sun, J. F. Bai, B. S. Zheng, Y. Z. Li, *Cryst. Growth Des.* **2012**, *12*, 1081 – 1084; c) R. Sun, Y.-Z. Li, J. Bai, Y. Pan, *Cryst. Growth Des.* **2007**, *7*, 890 – 894; d) R. Sun, S. Wang, H. Xing, J. Bai, Y. Li, Y. Pan, X. You, *Inorg. Chem.* **2007**, *46*, 8451 – 8453; e) K. Tang, R. Yun, Z. Lu, L. Du, M. Zhang, Q. Wang, H. Liu, *Cryst. Growth Des.* **2013**, *13*, 1382 – 1385; f) B. Zheng, J. Bai, J. Duan, L. Wojtas, M. J. Zaworotko, *J. Am. Chem. Soc.* **2011**, *133*, 748 – 751; g) B. Zheng, Z. Yang, J. Bai, Y. Li, S. Li, *Chem. Commun.* **2012**, *48*, 7025 – 7027.

[10] a) D. Li, H. Furukawa, H. Deng, C. Liu, O. M. Yaghi, D. S. Eisenberg, *Proc. Natl. Acad. Sci. USA* **2014**, *111*, 191 – 196; b) D. Peri, J. Ciston, F. Gandara, Y. Zhao, O. M. Yaghi, *Inorg. Chem.* **2013**, *52*, 13818 – 13820; c) P. Vairaprakash, H. Ueki, K. Tashiro, O. M. Yaghi, *J. Am. Chem. Soc.* **2011**, *133*, 759 – 761; d) J. Bonnefoy, A. Legrand, E. A. Quadrelli, J. Canivet, D. Farrusseng, *J. Am. Chem. Soc.* **2015**, *137*, 9409 – 9416.

[11] a) M. Eddaoudi, J. Kim, N. Rosi, D. Vodak, J. Wachter, M. O'Keeffe, O. M. Yaghi, *Science* **2002**, *295*, 469 – 472; b) O. M. Yaghi, M. O'Keeffe, N. W. Ockwig, H. K. Chae, M. Eddaoudi, J. Kim, *Nature* **2003**, *423*, 705 – 714; c) H. Furukawa, Y. B. Go, N. Ko, Y. K. Park, F. J. Uribe-Romo, J. Kim, M. O'Keeffe, O. M. Yaghi, *Inorg. Chem.* **2011**, *50*, 9147 – 9152.

[12] T. Devic, O. David, M. Valls, J. Marrot, F. Couty, G. Ferey, *J. Am. Chem. Soc.* **2007**, *129*, 12614 – 12615.

[13] a) J. Park, J. R. Li, Y. P. Chen, J. Yu, A. A. Yakovenko, Z. U. Wang, L. B. Sun, P. B. Balbuena, H. C. Zhou, *Chem. Commun.* **2012**, *48*, 9995 – 9997; b) P. Zhang, B. Li, Y. Zhao, X. Meng, T. Zhang, *Chem. Commun.* **2011**, *47*, 7722 – 7724.

[14] V. Guillerm, D. Kim, J. F. Eubank, R. Luebke, X. Liu, K. Adil, M. S. Lah, M. Eddaoudi, *Chem. Soc. Rev.* **2014**, *43*, 6141 – 6172.

[15] a) J. Lu, A. Mondal, B. Moulton, M. J. Zaworotko, *Angew. Chem. Int. Ed.* **2001**, *40*, 2113 – 2116; *Angew. Chem.* **2001**, *113*, 2171 – 2174; b) J. J. t. Perry, V. Kravtsov, G. J. McManus, M. J. Zaworotko, *J. Am. Chem. Soc.* **2007**, *129*, 10076 – 10077; c) A. J. Cairns, J. A. Perman, L. Wojtas, V. Kravtsov, M. H. Alkordi, M. Eddaoudi, M. J. Zaworotko, *J. Am. Chem. Soc.* **2008**, *130*, 1560 – 1561.

[16] a) H. Deng, S. Grunder, K. E. Cordova, C. Valente, H. Furukawa, M. Hmadeh, F. Gandara, A. C. Whalley, Z. Liu, S. Asahina, H. Kazumori, M. O'Keeffe, O. Terasaki, J. F. Stoddart, O. M. Yaghi, *Science* **2012**, *336*, 1018 – 1023; b) Y. Yan, S. Yang, A. J. Blake, W. Lewis, E. Poirier, S. A. Barnett, N. R. Champness, M. Schröder, *Chem. Commun.* **2011**, *47*, 9995 – 9997; c) X. Lin, I. Telepeni, A. J. Blake, A. Dailly, C. M. Brown, J. M. Simmons, M. Zoppi, G. S. Walker, K. M. Thomas, T. J. Mays, P. Hubberstey, N. R. Champness, M. Schröder, *J. Am. Chem. Soc.* **2009**, *131*, 2159 – 2171; d) T. Li, M. T. Kozlowski, E. A. Doud, M. N. Blakely, N. L. Rosi, *J. Am. Chem. Soc.* **2013**, *135*, 11688 – 11691.

[17] a) Y. Yan, X. Lin, S. Yang, A. J. Blake, A. Dailly, N. R. Champness, P. Hubberstey, M. Schröder, *Chem. Commun.* **2009**, 1025 – 1027; b) D. Zhao, D. Yuan, D. Sun, H. C. Zhou, *J. Am. Chem. Soc.* **2009**, *131*, 9186 – 9188; c) R. Grünker, V. Bon, A. Heerwig, N. Klein, P. Müller, U. Stoeck, I. A. Baburin, U. Mueller, I. Senkovska, S. Kaskel, *Chem. Eur. J.* **2012**, *18*, 13299 – 13303.

[18] a) N. Klein, I. Senkovska, K. Gedrich, U. Stoeck, A. Henschel, U. Mueller, S. Kaskel, *Angew. Chem. Int. Ed.* **2009**, *48*, 9954 – 9957; *Angew. Chem.* **2009**, *121*, 10139 – 10142; b) I. Senkovska, S. Kaskel, *Chem. Commun.* **2014**, *50*, 7089 – 7098; c) J. An, O. K. Farha, J. T. Hupp, E. Pohl, J. I. Yeh, N. L. Rosi, *Nat. Commun.* **2012**, *3*, 604; d) K. Wang, D. Feng, T. F. Liu, J. Su, S. Yuan, Y. P. Chen, M. Bosch, X. Zou, H. C. Zhou, *J. Am. Chem. Soc.* **2014**, *136*, 13983 – 13986; e) K. Koh, A. G. Wong-Foy, A. J. Matzger, *Angew. Chem. Int. Ed.* **2008**, *47*, 677 – 680; *Angew. Chem.* **2008**, *120*, 689 – 692.

[19] H. Furukawa, N. Ko, Y. B. Go, N. Aratani, S. B. Choi, E. Choi, A. O. Yazaydin, R. Q. Snurr, M. O'Keeffe, J. Kim, O. M. Yaghi, *Science* **2010**, *329*, 424 – 428.

[20] G. Ferey, C. Mellot-Draznieks, C. Serre, F. Millange, J. Dutour, S. Surble, I. Margiolaki, *Science* **2005**, *309*, 2040 – 2042.

[21] Y. S. Bae, K. L. Mulfort, H. Frost, P. Ryan, S. Punnathanam, L. J. Broadbelt, J. T. Hupp, R. Q. Snurr, *Langmuir* **2008**, *24*, 8592 – 8598.

[22] Z. Zhang, Z. Li, J. Li, *Langmuir* **2012**, *28*, 12122 – 12133.

[23] T. Li, D.-L. Chen, J. E. Sullivan, M. T. Kozlowski, J. K. Johnson, N. L. Rosi, *Chem. Sci.* **2013**, *4*, 1746 – 1755.

[24] a) J. A. Mason, K. Sumida, Z. R. Herm, R. Krishna, J. R. Long, *Energy Environ. Sci.* **2011**, *4*, 3030 – 3040; b) D. Saha, Z. Bao, F. Jia, S. Deng, *Environ. Sci. Technol.* **2010**, *44*, 1820 – 1826.

[25] Z. Zhang, Y. Zhao, Q. Gong, Z. Li, J. Li, *Chem. Commun.* **2013**, *49*, 653 – 661.

[26] B. Li, Z. Zhang, Y. Li, K. Yao, Y. Zhu, Z. Deng, F. Yang, X. Zhou, G. Li, H. Wu, N. Nijem, Y. J. Chabal, Z. Lai, Y. Han, Z. Shi, S. Feng, J. Li, *Angew. Chem. Int. Ed.* **2012**, *51*, 1412 – 1415; *Angew. Chem.* **2012**, *124*, 1441 – 1444.

[27] P. L. Llewellyn, S. Bourrelly, C. Serre, A. Vimont, M. Daturi, L. Hamon, G. De Weireld, J. S. Chang, D. Y. Hong, Y. Kyu Hwang, S. Hwa Jhung, G. Ferey, *Langmuir* **2008**, *24*, 7245 – 7250.

Received: December 5, 2015
Published online on March 31, 2016